IEEE Access
Multidisciplinary | Rapid Review | Open Access Journal

Received 14 April 2024, accepted 28 May 2024, date of publication 3 June 2024, date of current version 10 June 2024.

Digital Object Identifier 10.1109/ACCESS.2024.3408340

RESEARCH ARTICLE

A Noise Covariance Regulated Robust Modified Adaptive Extended Kalman Filter for State of Charge Estimation of Lithium-Ion Battery

SATYAPRAKASH ROUT, (Student Member, IEEE), AND SATYAJIT DAS
School of Electrical Engineering, VIT University, Vellore, Tamil Nadu 632014, India

Corresponding author: Satyajit Das (satyajit.das@vit.ac.in)

This work was supported by the School of Electrical Engineering, VIT University, Vellore, India.

ABSTRACT A battery management system needs a robust algorithm for online state-of-charge estimation of batteries in different dynamic systems. Due to the ease of implementation, model-based state-of-charge estimation using the extended Kalman filter is popularly used in battery management systems for online state-of-charge estimation. However, the accuracy of the extended Kalman filter depends on the appropriate initialization of noise covariance. In this paper, a robust modified adaptive extended Kalman filter (RMAEKF) is proposed that enhances the state-of-charge estimation accuracy by incorporating recursive adaptive correction rules for process and measurement noise covariance matrices. The adaptive rule considers the predicted terminal voltage error and the state prediction error in each time step to provide the necessary correction of measurement noise covariance and process noise covariance respectively. Further, to validate the state-of-charge estimation accuracy of the proposed RMAEKF, its performance indices for LA92, US06, and mixed drive cycles are obtained at different operating temperatures and compared with the performance indices of the extended Kalman filter and forgetting factor-based adaptive extended Kalman filter. Moreover, the robustness of the proposed RMAEKF is examined with different initial values of state-of-charge, noise covariance matrices, offset current and bias voltage. In addition to that, an experiment using the OPAL-RT real-time simulator is also performed to validate the proposed methodology for online SOC estimation. Concurrently, mean execution time and computational complexity analyses of the proposed RMAEKF are performed to check its applicability in real-time battery management system applications. From the result analysis, it is observed that the proposed RMAEKF shows better robustness and higher state-of-charge estimation accuracy than other compared algorithms under dynamic operating conditions.

INDEX TERMS Adaptive noise correction, battery electric vehicle, battery management system, state-of-charge.

I. INTRODUCTION

Increasing demand for electrical energy generation is attracting researchers to look for low-carbon, clean, and sustainable energy sources like solar energy, wind energy, bio-energy, etc. The electricity generated from the aforesaid sources needs a storage device or battery for future utilization. Recently, lithium-ion or polymer batteries got more attention due to their long life cycle, low maintenance, no memory effect, low self-discharge rate, and high specific energy density [1], [2]. In spite of all these advantages, lithium-ion or polymer batteries are expensive as compared to lead-acid and nickel-metal hybrid batteries and possess complicated chemical dynamics during the charging and discharging process. Due to this, it is difficult to assume the internal state of the battery during operating conditions. To ensure the safe and reliable operation of battery-powered systems, an efficient battery management system (BMS) is essential that can accurately estimate the internal state of the battery. BMS measures all the essential parameters of the battery or battery pack

The associate editor coordinating the review of this manuscript and approving it for publication was Enamul Haque.

for handling thermal degradation and cell balancing. It also senses the temperature, measures terminal voltage, battery current, and different states of the battery during on-load conditions [3]. The state-of-charge (SOC) of the battery gives an indication of the available useful energy left for utilization with respect to the rated capacity of the battery. However, SOC cannot be measured directly but can only be estimated by observing the current, voltage, and operating temperature of the battery. The service life of the battery can be enhanced by operating it within a certain range of SOC. Hence, accurate estimation of SOC becomes an important task in all battery-dependent systems, such as battery electric vehicles (BEVs) and hybrid electric vehicles (HEVs). Electric vehicles (EVs) have a very dynamic power demand profile. So, BMS should have a robust and accurate online SOC estimation technique to deal with such a dynamic operating condition.

A. LITERATURE SURVEY

In recent times, many SOC estimation techniques have been developed, such as the coulomb-counting method (CCM), the model-based estimation method (MEM), and the data-driven method (DDM). [4]. However, due to its ease of implementation, the MEM is widely used for SOC estimation in BMS applications [5]. For MEM, many equivalent models of batteries are proposed, such as the empirical model (EM), the electrochemical impedance model (EchIM), and the equivalent circuit model (ECM) [4]. Compared to other models, ECM is easy to implement in embedded electronics systems with acceptable modeling accuracy and moderate computation complexity. ECM consists of a voltage source connected in series with a resistor and with a number of resistor-capacitor (RC) parallel branches to represent the cell dynamics [6], [7]. It is found that, with moderate computational stress on the estimation process, the 1-RC and 2-RC models with KF-based SOC estimation algorithms show good accuracy in SOC estimation.

Recently, many variants of KF, such as the extended Kalman filter (EKF) [8], the unscented Kalman filter (UKF) [9], the cubature Kalman filter (CKF) [10], [11], and the sigma-point Kalman filter (SPKF) [12], were proposed for online SOC estimation of the battery. Out of which, EKF shows a good trade-off between estimation accuracy and computational complexity among other advanced variants of KF. However, the performance of the KF is contingent upon the accuracy of the noise statistics. This requires an adaptive extended Kalman filter (AEKF) capable of performing adaptive correction of the noise covariance matrix (NCM) in accordance with the change in state prediction error and innovation. Article [1] proposed an affine iterative AEKF that considers non-Gaussian white noise and estimates the innovation covariance matrix (ICM) using a sliding window technique with a fixed window size. In [13], the NCM is updated using Sage-Husa adaptive filtering, and the ICM is modified using the variable sliding window technique with upper and lower threshold values taken into account. Furthermore, [13] analyzed the actual and theoretical ICMs in order to create an adaptive correction factor for updating the predicted state error covariance matrix (SECM). Adaptive correction of SECM significantly enhances SOC estimation precision. Similarly, in order to identify the ICM, [14] employed the variable sliding window technique by considering the change in error innovation sequence (EIS) in each iteration. Consideration of the EIS seems more persuasive than consideration of a specific threshold value. The implementation of the sliding window technique improves the SOC estimation accuracy, but at the expense of an increase in computational burden. To minimize the computational burden during SOC estimation with the sliding window method, [15], [16] proposed a forgetting factor-based AEKF (FFAEKF) that includes a weighted coefficient to update the noise matrices. Reference [15] determines the innovation and residual of estimated terminal voltage using posterior and prior SECM, whereas [16] used posterior and prior estimates for the determination of innovation and residual of estimated terminal voltage. The comparative statistical analysis infers that FFAEKF-II, proposed in [15], has better estimation accuracy than FFAEKF-I, which is proposed in [16]. In FFAEKF, the inclusion of the forgetting factor provides more fluctuation to Kalman gain during SOC estimation by emphasizing the most recent data samples, which reduces the computational burden of the overall SOC estimation process. However, selecting the appropriate forgetting factor value can be a burdensome task. To resolve this issue, [17] incorporated a fuzzy logic controller for the selection of forgetting factors. However, the implementation of a fuzzy logic controller for determining the forgetting factor increases the computational complexity and memory requirements. Though the incorporation of the forgetting factor enhances the SOC estimation accuracy, the performance of FFAEKF under the influence of operating temperature variation, measurement bias, and improper initialization of noise covariance matrices were not examined. These aforementioned operating conditions may reduce the robustness of the estimation algorithm.

B. PROBLEM FORMULATION

In the model-based estimation, a non-linear dynamic system is represented by the following state space model:

$$S_k = g(S_{k-1}, c_{k-1}) + p_{k-1} \tag{1}$$

$$O_k = h(S_k, c_k) + m_k \tag{2}$$

where c_k is the known input control variable, S_k is the unknown model state vector, O_k is the measured output of the system, $p_k \sim N(0, P_k)$ represents the unknown and immeasurable process noise vector with zero mean and covariance P_k, and $m_k \sim N(0, M_k)$ represents the measurement noise vector with zero mean and covariance M_k. KF has mainly two runtime processes, i.e., prediction and correction. The prediction process can be expressed as

follows:

$$\hat{S}_{k|k-1} = G_{k-1}\hat{S}_{k-1|k-1} + H_{k-1}c_{k-1} \quad (3)$$

$$E_{k|k-1} = G_{k-1}\hat{E}_{k-1|k-1}G_{k-1}^T + P_{k-1} \quad (4)$$

where $S_{k|k-1}$ and $E_{k|k-1}$ are the predicted state vector matrix (SVM) and predicted state error covariance matrix, G_{k-1} is the state transition matrix, and P_k is the process noise covariance matrix. In the next step, the KF updates the predicted SVM and SECM as follows:

$$\hat{O}_k = W_k\hat{S}_{k|k-1} + V_k c_k \quad (5)$$

$$z_k = O_k - \hat{O}_k \quad (6)$$

$$Z_k = E[z_k z_k^T] = W_k E_{k|k-1}W_k^T + M_k \quad (7)$$

$$K_k = E_{k|k-1}W_k^T Z_k^{-1} \quad (8)$$

$$\hat{S}_{k|k} = \hat{S}_{k|k-1} + K_k z_k \quad (9)$$

$$E_{k|k} = (I - K_k W_k)E_{k|k-1} \quad (10)$$

where $\hat{O}_k$ is the predicted output, z_k gives the predicted output error or innovation, W_k is the output state transition matrix, Z_k is the ICM, K_k is the Kalman gain, and M_k is the measurement noise covariance matrix.

The standard EKF algorithm leverages the noise statistics to modulate the Kalman gain, which is subsequently employed to correct the filter innovation error [18]. This adjustment leads to the refinement of the process information, ultimately resulting in an improved estimation. However, the stability and reliability of the EKF are contingent upon the accurate estimation of the parameters of the stochastic battery model [19]. In EKF-based SOC estimation, the modeling uncertainty caused by the linearization of the non-linear battery model is represented by the process noise covariance matrix (PNCM). Inaccurate initialization of PNCM in EKF may lead to filter divergence. Similarly, in EKF measurement, the noise covariance matrix (MNCM) represents the uncertainty in estimation due to noisy measurement. Inaccurate initialization of MNCM in EKF leads to inaccuracy in SOC estimation and reduces the filter convergence speed.

In practice, batteries work under uncertain operating conditions, which affect their physical and chemical characteristics. In addition to that, noise in sensor measurement during on-load conditions may result in inappropriate Kalman gain for the EKF algorithm. Hence, the selection of fixed values of P and M may degrade accuracy in SOC estimation under dynamic operating conditions. The aforementioned limitations demand an adaptive extended Kalman filter (AEKF) with adaptive correction of P and M matrix elements in each time step for an accurate state estimation. Moreover, the adaptive algorithm needs to be computationally efficient and robust enough to be implemented on a BMS for real-time operation. Therefore, a robust modified adaptive extended Kalman filter (RMAEKF) is proposed in this work.

C. CONTRIBUTION OF THE WORK

In order to address the aforementioned problems in SOC estimation, a noise covariance regulated modified AEKF is proposed in this article. In the proposed RMAEKF process and measurement noise covariance matrix are regulated with state prediction error and change in innovation sequence respectively. The contributions made in this article are as follows:

- An adaptive correction factor is designed by considering the estimated state error and mean state error covariance in each time step to update the PNCM. The adaptive design of PNCM enhances the robustness of the filter during parametric uncertainty due to the variation in battery operating temperature.
- The design of adaptive MNCM incorporates a correction factor by evaluating the difference between the actual innovation covariance matrix and the theoretical innovation covariance matrix in each iteration. The aforesaid adaptive tuning of Kalman filter gain increases the convergence speed and provides high SOC estimation accuracy in the presence of offset current and bias voltage in sensor measurement.
- The mean execution time and worst-case computational complexity of the proposed RMAEKF are evaluated to ensure cost effectiveness in practical BMS applications.
- Finally, the efficacy of the proposed RMAEKF in SOC estimation is validated by performing an OPAL-RT based real-time simulation.

D. ORGANIZATION OF THE PAPER

The rest of the article is organized as follows: Section II describes the 2-RC ECM architecture and battery parameter identification procedures. In Section III, the steps of the proposed SOC estimation technique are elaborated briefly. The details of the experimental setting and the test data set used in this work are reported in Section IV. Section V shows the comparative result analysis, computation time, and computational complexity analysis of the proposed work. Section VI describes the details of the real-time experimentation performed and its corresponding result analysis. Finally, the conclusion is specified in Section VII.

II. BATTERY MODEL ARCHITECTURE AND SOC DEFINITION

Fig.1 represents the equivalent circuit model (ECM) of the battery, where R_0 is the internal resistance of the battery. The two parallel RC branches, i.e., R_{st}, C_{st} and R_{lt}, C_{lt} represent the short-duration and long-duration transient effects, respectively. V_{oc} is the open circuit voltage as a function of SOC and temperature, and V_t represents the terminal voltage of the battery. V_1 and V_2 are the polarization voltages across $R_{st}C_{st}$ and $R_{lt}C_{lt}$, respectively. I_B is the battery current and is considered to be $+ve$ during discharging and $-ve$ during charging.

Applying Krichhoff's voltage law to the circuit depicts in Fig.1, the terminal voltage can be represented as follows

$$V_t = V_{oc}(SOC, T) - V_1 - V_2 - I_B R_0 \quad (11)$$

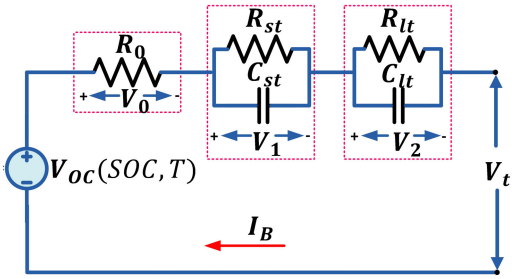

FIGURE 1. Equivalent circuit model (2)-RC model) of battery.

where V_1 and V_2 expressed as

$$\dot{V_1} = -\frac{V_1}{R_{st}C_{st}} + \frac{I_B}{C_{st}} \tag{12}$$

$$\dot{V_2} = -\frac{V_2}{R_{lt}C_{lt}} + \frac{I_B}{C_{lt}} \tag{13}$$

State of charge (SOC) can be accurately calculated using open loop Ampere-hour integral (AHI) [5] method as given in (14)

$$SOC_t = SOC_0 - \int_{t_0}^{t} \frac{\eta I_B(t)dt}{C_B} \tag{14}$$

where SOC_0 is the initial SOC, t_0 is the initial time, η is the coulombic efficiency, C_B is the battery nominal capacity.

In this work SOC, V_1 and V_2 are considered as the unknown states that needs to be estimated. The state space model representation of ECM can be described as

$$\begin{bmatrix} \mathrm{SOC_{k+1}} \\ V_{1,k+1} \\ V_{2,k+1} \end{bmatrix} = \begin{bmatrix} 1 & 0 & 0 \\ 0 & \exp^{\frac{-\Delta T}{R_{st}C_{st}}} & 0 \\ 0 & 0 & \exp^{\frac{-\Delta T}{R_{lt}C_{lt}}} \end{bmatrix} \begin{bmatrix} \mathrm{SOC_k} \\ V_{1,k} \\ V_{2,k} \end{bmatrix} + \begin{bmatrix} -\frac{\Delta T}{C_B}\eta_k \\ R_{st}\left(1-\exp^{\frac{-\Delta T}{R_{st}C_{st}}}\right) \\ R_{lt}\left(1-\exp^{\frac{-\Delta T}{R_{lt}C_{lt}}}\right) \end{bmatrix} [I_{B,k}] \tag{15}$$

$$[V_{t,k}] = \begin{bmatrix} \frac{\partial V_{OC}}{\partial SOC} & -1 & -1 \end{bmatrix} \begin{bmatrix} \mathrm{SOC_k} \\ V_{1,k} \\ V_{2,k} \end{bmatrix} + [-R_0][I_{B,k}] \tag{16}$$

where ΔT is the sample time.

A. SOC VS. OCV CURVE

The open circuit voltage (OCV) of the battery can't be measured directly; hence it is approximated by knowing the corresponding SOC value. The SOC-OCV relation for a particular operating temperature is obtained by performing low current test that keep the cell in equilibrium state all time. In low current test, the fully charge battery (SOC = 100%) is slowly discharged with a C-rate of C/20 to its cutoff voltage value (SOC = 0%) followed by slowly charging the battery to its maximum operating voltage. Lastly, the obtained charging and discharging SOC-OCV curve is averaged to obtain the required SOC-OCV curve for a given operating temperature. The SOC-OCV curve for 0^0C, 25^0C and 40^0C is shown in Fig.2.

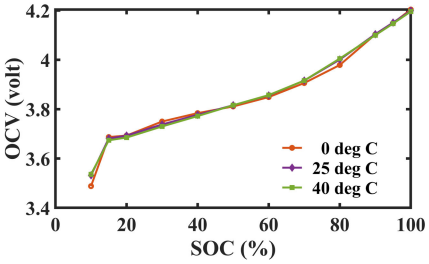

FIGURE 2. SOC-OCV curve at 0^0C, 25^0C and 40^0C.

B. BATTERY MODEL PARAMETER IDENTIFICATION

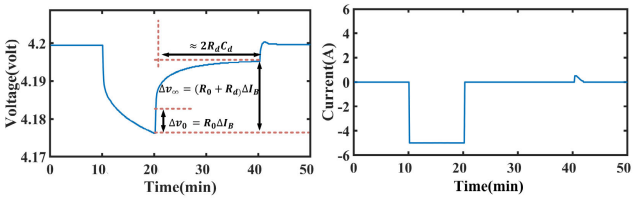

FIGURE 3. a) Parameter identification from a pulse response b) corresponding current.

In model-based SOC estimation, the accuracy of the predicted state value depends significantly upon the battery model parameters [20]. The internal state of a lithium battery (LIB) is affected by the cell chemistry, ambient temperature, and residual capacity of the battery. Hence, the battery model parameter changes with variations in operating temperature, C-rate, charge / discharge cycle, and SOC of the battery [21]. One of the most common methods of parameter identification is offline calculation of battery model parameters. In offline parameter estimation, the battery is subjected to a hybrid pulse power characterization (HPPC) test at different operating temperatures [7].

Fig.3a & 3b shows the voltage and current for the first pulse response obtained from the HPPC test. In Fig.3a, Δv_0 represents the instantaneous change in voltage when pulse current is removed and Δv_∞ represents the steady state voltage response. Similarly, ΔI_B is the change in battery current and R_d C_d represents diffusion resistance and capacitance respectively. Referring to Fig.3a the internal resistance R_0 and diffusion resistance R_d can be found using (17) & (18) respectively.

$$R_0 = \left| \frac{\Delta v_0}{\Delta I_B} \right| \tag{17}$$

$$R_d = \left| \frac{\Delta v_\infty}{\Delta I_B} \right| - R_0 \tag{18}$$

Furthermore, it can be observed that the voltage converges to a steady state in about 20 minutes. Considering the

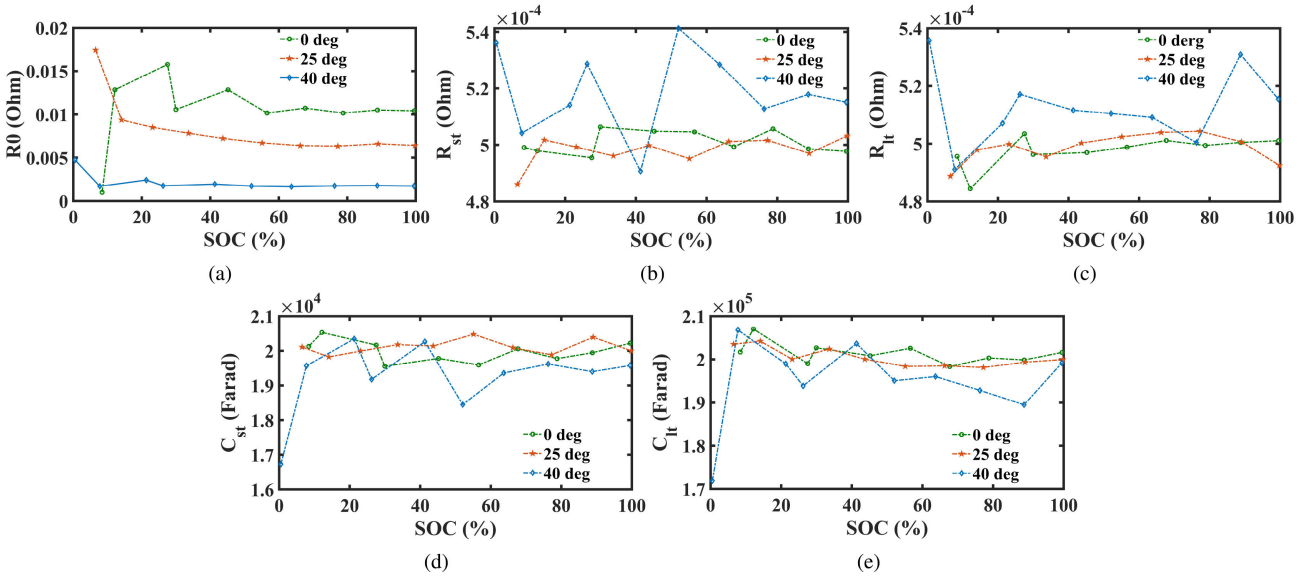

FIGURE 4. Battery parameters with respect to variation in SOC at 0^0C,25^0C and 40^0C: (a) R_0,(b) R_1,(c) R_2, (d) C_1 and (e) C_2.

time constant of the RC circuit, C_d can be calculated. However, considering the real-time application, it is essential to estimate the battery model parameter online. In this proposed work, a new 5Ah Turnigy cell (Turnigy Graphene 5000mAh 65C cell) is used to perform an HPPC test [22], and the obtained test data is processed in MATLAB / Simulink-based model-based parameter optimization at different temperatures as a function of SOC. The obtained ECM parameter values of the battery are then determined in each iteration using the *scatteredInterpolant* function of MATLAB, as discussed in [23] and [24]. The results of the identified battery parameters for different SOCs at 0^0C, 25^0C, and 40^0C temperatures are shown in Fig.4. It is observed that the discharge capacity of LIB reduces at low temperatures and increases at high operating temperatures. Further, li-ion batteries have fast electrolyte response in high operating temperatures and slow electrolyte response at low operating temperatures due to variation in battery internal resistance [25]. The aforesaid reason leads to change in battery parameters with respect to changes in SOC and temperature, which can be observed from Fig.4.

III. PROPOSED METHOD FOR SOC ESTIMATION

This section explains the design of adaptive rules that are incorporated in the proposed RMAEKF. The working structure of the proposed SOC estimation method is shown in Fig.5. The process and measurement noise are corrected using the adaptive rule as discussed below.

A. ADAPTIVE NOISE COVARIANCE UPDATE RULES

From Section I-B, it is clear that the accuracy of a KF-based state estimator degrades when the noise covariance matrix values are too large or too small relative to their true value. Hence, two recursive noise correction rules $Rule-I$ and $Rule-II$ are incorporated in the proposed RMAEKF to update both P and M adaptively in order to achieve better accuracy in SOC estimation. For the given non-linear dynamic system in Eq.1 & 2 the SOC estimation is carried out by considering the following assumptions:

Assumption1: Process noise (p_k) and measurement noise (m_k) are assumed to be independent and uncorrelated to each other, i.e., $E(p_k) = E(m_k) = E(pm^T) = 0$. Where E(.) represents the expected value of (.).

Assumption2: The input current I_B is considered to have a sample time interval of T, i.e $I_B(t) = I_{B,k-1}$, $t_{k-1} \leq t < t_k$. Where $t_k = t_{k-1} + T$. further, both p_k and m_k should have same sampling time interval.

With the above mentioned assumption, for a given initial value of P_0 and M_0 the proposed RMAEKF incorporates two positive constants C_P and C_M and the noise covariance error ΔP and ΔM to update the noise covariance matrices recursively utilizing the following rules [26].

- **Initialization**:

$$\bar{d}_0, \bar{z}_0, \hat{S}_0, E_0 > 0, P_0 > 0, M_0 > 0 \tag{19}$$

- **Rule-I: For Process noise covariance correction**

$$\beta_1 = \frac{C_P - 1}{C_P} \tag{20}$$

$$\hat{d}_k = \hat{S}_{k|k} - \hat{S}_{k|k-1} \tag{21}$$

$$\bar{d}_k = \beta_1 \bar{d}_{k-1} + \frac{1}{C_P}\hat{d}_k \tag{22}$$

$$\Delta P_k = \frac{1}{C_P - 1}\left(\hat{d}_k - \bar{d}_k\right)\left(\hat{d}_k - \bar{d}_k\right)^T + \frac{1}{C_P}\left(E_{k|k-1} - G_k E_{k-1|k-1} G_k{}^T\right) \tag{23}$$

$$P_k = \mid diag\left(\beta_1 P_{k-1} + \Delta P_k\right) \mid \tag{24}$$

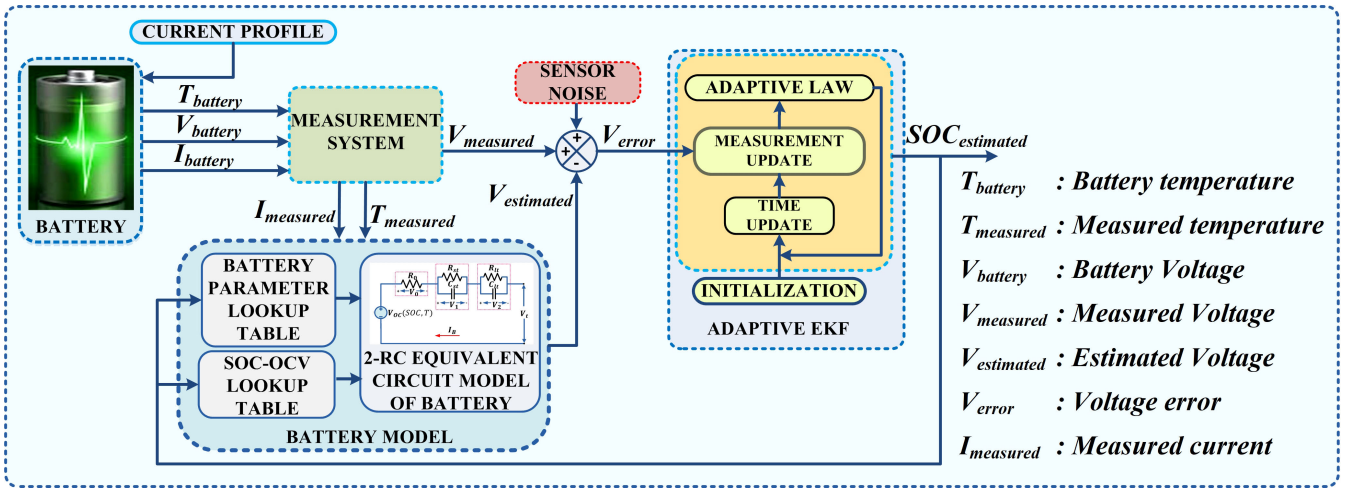

FIGURE 5. Working structure of proposed SOC estimation.

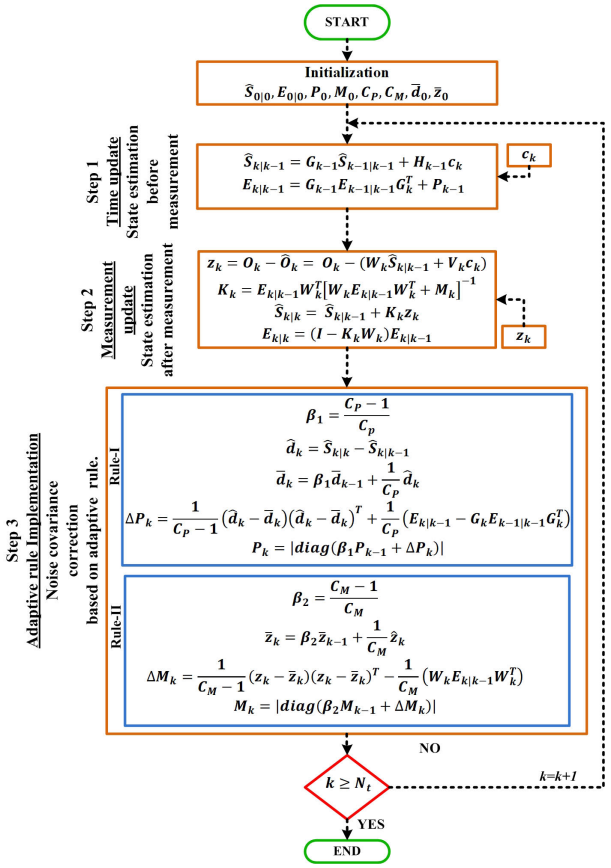

FIGURE 6. Flowchart of proposed RMAEKF.

- **Rule-II: For measurement noise covariance correction**

$$\beta_2 = \frac{C_M - 1}{C_M} \tag{25}$$

$$\bar{z}_k = \beta_2\bar{z}_{k-1} + \frac{1}{C_M}z_k \tag{26}$$

$$\Delta M_k = \frac{1}{C_M - 1}(z_k - \bar{z}_k)(z_k - \bar{z}_k)^T - \frac{1}{C_M}W_k E_{k|k-1}W_k^T \tag{27}$$

$$M_k = |\, diag\,(\beta_2 M_{k-1} + \Delta M_k)\,| \tag{28}$$

where $\hat{d}_k$ is the state prediction error and z_k is the output prediction error.

From (24) and (28) it can be observed that the rule used to update noise covariance matrices always keeps the P_k and M_k matrix as positive definite for all k. Here, to add more flexibility to the noise covariance update rule, the value of C_P and C_M are user defined based on the system noise characteristics. These two positive constants can be set to have a big value for a noisy system or a smaller value for a less noisy system without losing generality. Furthermore, the proposed adaptive rule reduces computational burden as the noise covariance matrices can be updated only by tuning C_P and C_M value instead of tuning all the diagonal elements.

B. PROOF OF ADAPTIVE COVARIANCE UPDATE RULE

To prove the proposed Rule-I and II as discussed in Section III-A, the true value of state and the actual value of terminal voltage need to be known. However, during online SOC estimation only the sensor measured battery terminal voltage is known. Hence, the proof of measurement noise covariance update rule is illustrated first. In EKF, estimated terminal voltage can be evaluated as per (5) and (16). Now considering the predicted output voltage and actual terminal voltage, one can find the predicted output error covariance as per (7). In (7), M_k is the assumed value of MNCM and considered to be constant. Suppose there exists an uncertainty in M and let it be termed as ΔM. Then (7) can be rewritten as

$$Z_k = W_k E_{k|k-1}W_k^T + M_k - \Delta M \tag{29}$$

Now, ΔM value can be determined from (6) as it gives the information regarding the innovation. For a set number C_M of output observations, the mean and covariance of the output

terminal voltage can be described as

$$\bar{z}_k = \frac{1}{C_M}\sum_{i=1}^{C_M} z_i \tag{30}$$

$$\Delta M = \frac{1}{C_M - 1}\sum_{i=1}^{C_M}(z_i - \bar{z}_i)(z_i - \bar{z}_i)^T \tag{31}$$

Putting the value of ΔM from (31) in to (29) and performing mathematical simplification M can be obtained as

$$M = \frac{1}{C_M - 1}\sum_{i=1}^{C_M}(z_i - \bar{z}_i)(z_i - \bar{z}_i)^T - \frac{1}{C_M}\left(\sum_{i=1}^{C_M}(W_k E_{k|k-1} W_k^T)_i\right) \tag{32}$$

(32) indicates that the MNC are updated in each time index, which infers the correlation between the present and previous covariance samples. This relationship between the recent noise covariance can be found by separating them into two groups i.e., group-1 containing covariance from $i = k - C_M$ to $i = k - 1$ and group-2 containing only the covariance at time k. Further, after a few mathematical manipulation, the sample covariance in group-1 can be approximated with a large value of C_M as

$$\frac{C_M}{(C_M - 1)^2} \times \sum_{i=k-C_M}^{k-1}(z_i - \bar{z}_i)(z_i - \bar{z}_i)^T \tag{33}$$

and (32) can be expressed as

$$M_k = \frac{C_M - 1}{C_M} M_{k-1} + \Delta M_k \tag{34}$$

$$M_{k-1} \approx \frac{1}{C_M - 2}\sum_{i=k-C_M}^{k-1}(z_i - \bar{z}_i)(z_i - \bar{z}_i)^T - \left(\frac{1}{C_M - 1}\sum_{i=k-C_M}^{k-1}(W_k E_{k|k-1} W_k^T)_i\right) \tag{35}$$

$$\Delta M_k = \frac{1}{C_M - 1}(z_k - \bar{z}_k)(z_k - \bar{z}_k)^T - \frac{1}{C_M}\left(W_k E_{k|k-1} W_k^T\right) \tag{36}$$

As shown above, (34) implies the proof of adaptive rule of MNCM as given in (28).
Using the same methodology $\bar{z}_k$ can be computed as

$$\bar{z}_k = \frac{1}{C_M}\sum_{i=k-C_M}^{k} z_i = \frac{1}{C_M}\sum_{i=k-C_M}^{k-1} z_i + \frac{1}{C_M} z_k \tag{37}$$

which can be reduced to

$$\bar{z}_k = \frac{C_M - 1}{C_M}\bar{z}_{k-1} + \frac{1}{C_M} z_k \tag{38}$$

In the same manner, the adaptive rule for PNCM can also be proved by using the same approximation and initiating the derivation by considering the SECM as expressed in (4) along with the one-step state prediction error as given in (21). Moreover, as the true value of state is unknown, so the initialized state value can be considered to start the derivation of the adaptive rule for PNCM. The flowchart of the proposed RMAEKF is shown in Fig.6.

IV. EXPERIMENTAL SETTINGS AND DATA SET REQUIREMENT

A. EXPERIMENTAL SPECIFICATION

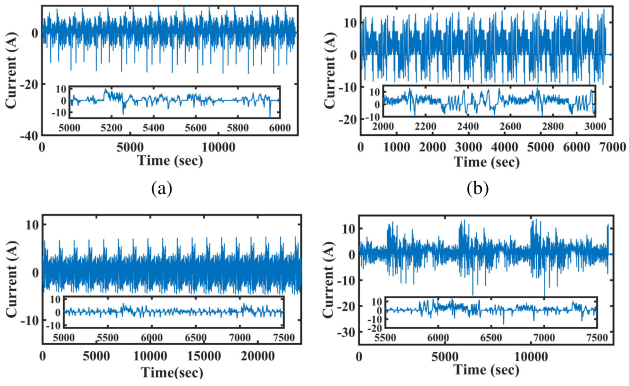

FIGURE 7. Dynamic load current profile of a) LA92, b) US06 c) UDDS and d) Mixed at 25^{0}C.

In order to check the efficacy of the proposed RMAEKF, a fully charged 5Ah Turnigy Graphene battery is considered, whose specifications are listed in Table-1. The battery model parameters are obtained by performing a four-pulse discharge HPPC test at 1, 2, 5, and 10 C-rate for both charging and discharging current, with a reduced value at low temperatures. The tests were carried out by covering the SOC range from 100% to 5% with an interval of 5%. After completion of each test, the battery is further charged at a 1C rate to 4.2V with a 5mA cut-off charge current at room temperature. [22].

TABLE 1. Battery specification.

Items	Values
Nominal Voltage	3.7 V
Charge	4.2 V, 5mA End-Current (CC-CV) Fast
Discharge	2.8 V End Volatge, 20A MAX Continous Current
Nominal Capacity	5 Ah
Energy Density	134 (Wh/Kg)

Once all the required battery test data sets are prepared, the proposed algorithm is processed in a MATLAB / SIMULINK environment. Here, the SOC calculated by the coulomb counting method is considered the reference SOC. The proposed online SOC estimation process began with the initialization of state, state covariance, noise covariance, and simulation parameters as mentioned in Table-2. To examine the estimation accuracy, the current profiles of three different drive cycles, i.e., LA92, US06, UDDS, and mixed drive cycles at 0^{0}C, 25^{0}C and 40^{0}C operating temperatures are considered in this work. The dynamic current profile of LA92, US06, UDDS, and mixed drive cycles at 25^{0}C is

TABLE 2. Initialization and simulation parameters.

Parameters	Values
Sample time (ΔT)	1sec
Initial SOC ($S_{0\|0}$)	100%
$E_{0\|0}$	$10^{-2}I_{3\times3}$
C_P	10
C_M	3×10^5
$\bar{d}_0$	$0_{3\times3}$
$\bar{z}_0$	0
P_0	$10^{-3}I_{3\times3}$
P_{small}	$10^{-5}I_{3\times3}$
P_{big}	$10^{-2}I_{3\times3}$
M_0	10^{-2}
M_{small}	2×10^{-3}
M_{big}	0.1

shown in Fig.7 for reference. LA92 is a drive cycle that has high acceleration with less ideal time and is used for light-duty vehicles. Similarly, US06 represents high-acceleration and high-speed drive cycle where as, UDDS represents city driving condition. Both US06 and UDDS drive cycles are developed by the US Environment Protection Agency (EPA) for aggressive driving studies. [15]. Apart from that, a mixed drive cycle consisting of random mix of LA92, US06, HWFET, and UDDS is also considered in this work to check the robustness of the proposed RMAEKF under different working currents. In order to check the accuracy of SOC estimation, the performance indices of the proposed RMAEKF are compared with performance indices of EKF [27], FFAEKF-I [16] and FFAEKF-II [15] under the influence of variable operating temperatures, the improper initialization of noise covariance, and the sensor measurement bias. In this work, influence of incorrect initialization and presence of sensor measurement bias during SOC estimation is analyzed for 25^0C operating temperature. Moreover, the current profile of Mixed drive cycle is used for detailed analysis of SOC estimation result during the aforementioned malicious working conditions.

B. EVALUATION INDEX FOR PERFORMANCE ANALYSIS

In this article, root mean square error (*RMSE*) and maximum absolute error (*MAE*) are considered as the evaluation criteria to reflect the accuracy in SOC estimation of the proposed RMAEKF. *RMSE* represents the standard deviation of the difference between the true and estimated value of SOC to evaluate the estimation accuracy of an algorithm [17]. Similarly, *MAE* reflects the error in predicted SOC by computing the absolute error between the true and estimated values of SOC. The *RMSE* and *MAE* for predicted SOC can be expressed as shown in (39) and (40) respectively.

$$RMSE = \sqrt{\frac{1}{N}\sum_{i=1}^{N}[(SOC_{True})_k - (SOC_{Estimated})_k]^2} \quad (39)$$

$$MAE = max\,|(SOC_{True})_k - (SOC_{Estimated})_k| \quad (40)$$

In this work, the *RMSE* and *MAE* of the proposed RMAEKF, EKF, FFAEKF-I and FFAEKF-II are evaluated to check the SOC estimation accuracy, and a detailed comparative analysis is reported in Section V.

V. COMPARATIVE RESULT ANALYSIS

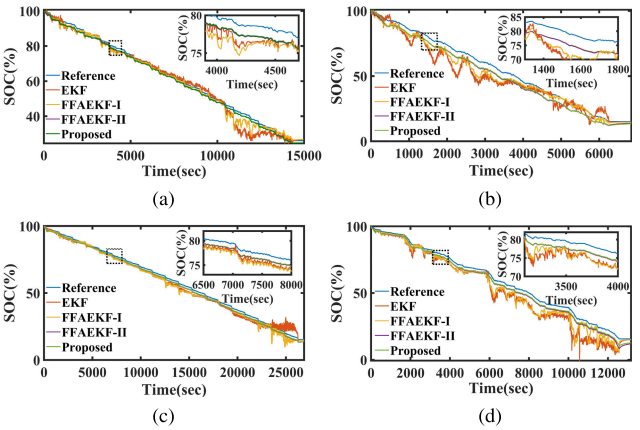

FIGURE 8. Estimated SOC result: (a) LA92,(b) US06 (c) UDDS and (d) Mixed drive cycle at 0^0C.

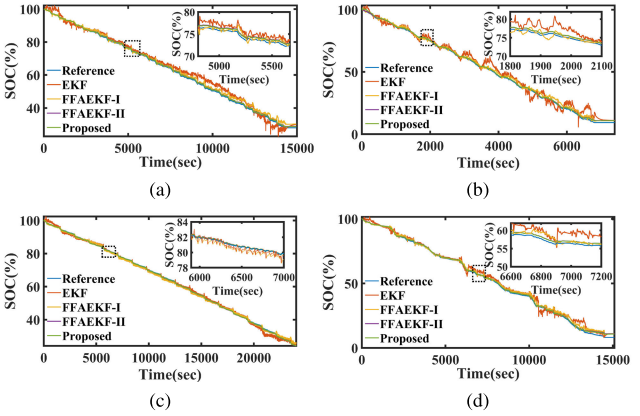

FIGURE 9. Estimated SOC result: (a) LA92,(b) US06 (c) UDDS and (d) Mixed drive cycle at 25^0C.

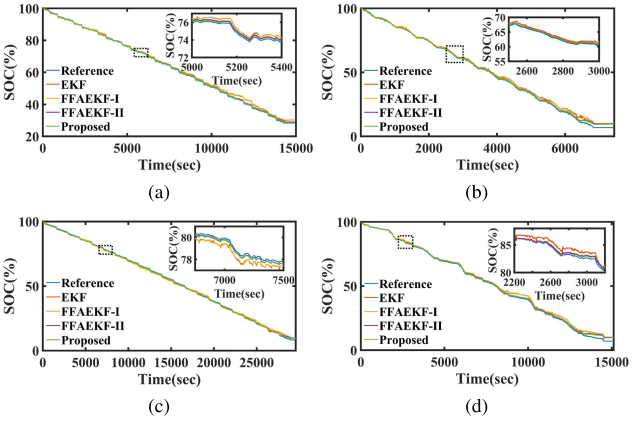

FIGURE 10. Estimated SOC result: (a) LA92,(b) US06 (c) UDDS and (d) Mixed drive cycle at 40^0C.

In this section, the estimation accuracy of the proposed RMAEKF is analyzed by comparing its RMSE and MAE

TABLE 3. Statistical result analysis of SOC estimation at 0^0C, 25^0C and 40^0C.

Current Profile	Methods	0^0C		25^0C		40^0C	
		RMSE (%)	MAE (%)	RMSE (%)	MAE (%)	RMSE (%)	MAE (%)
LA92	EKF	3.544	13.95	2.572	8.514	1.880	0.616
	FFAEKF-I	2.463	11.31	1.620	1.750	1.160	0.505
	FFAEKF-II	1.532	2.153	0.817	0.532	0.363	0.388
	Proposed	**1.370**	**1.941**	**0.506**	**0.122**	**0.270**	**0.315**
US06	EKF	7.351	30.71	3.436	10.10	1.844	0.912
	FFAEKF-I	4.960	13.91	1.786	2.239	1.786	0.559
	FFAEKF-II	4.287	5.232	0.897	0.569	1.089	0.372
	Proposed	**3.954**	**4.808**	**0.778**	**0.042**	**0.928**	**0.354**
Mixed	EKF	7.777	30.71	2.446	7.333	1.845	0.640
	FFAEKF-I	6.099	23.40	1.786	1.444	1.797	0.553
	FFAEKF-II	2.915	7.289	1.010	0.368	1.097	0.290
	Proposed	**2.472**	**5.145**	**0.881**	**0.287**	**0.925**	**0.199**
UDDS	EKF	2.751	7.628	0.968	4.509	0.860	1.505
	FFAEKF-I	2.679	13.03	0.836	1.870	0.903	1.289
	FFAEKF-II	1.527	2.048	0.298	0.403	0.463	0.451
	Proposed	**1.398**	**1.924**	**0.241**	**0.310**	**0.392**	**0.386**

with EKF, FFAEKF-I, and FFAEKF-II. Further, the efficacy and robustness of the proposed RMAEKF is examined under erroneous initialization of state and noise covariance. Moreover, the computational cost and matrix operation complexity analysis of proposed RMAEKF, EKF and FFAEKF (I & II) are analyzed to check the efficacy in SOC estimation. Apart from that the effectiveness of the proposed RMAEKF for SOC estimation is examined in the presence of offset current and bias voltage. The detailed analysis is reported as follows.

A. SOC ESTIMATION AT DIFFERENT TEMPERATURE

Fig.8, 9, and 10 shows the estimated SOC obtained by EKF, FFAEKF-I, FFAEKF-II and Proposed RMAEKF under the current profile of LA92, US06, UDDS and mixed drive cycle at 0^0C, 25^0C and 40^0C operating temperatures. The performance indices of the obtained SOC estimation results are listed in Table-3. From Table-3, it is observed that the proposed RMAEKF gives better estimation accuracy as compared to EKF, FFAEKF-I and FFAEKF-II with a comparatively minimum RMSE of 1.370%, 3.954%, 1.398% and 2.472% for LA92, US06, UDDS and mixed drive cycle respectively, at 0^0C. Similarly, the least MAE values of proposed RMAEKF i.e. 1.941%, 4.808%, 1.924% and 5.145% for LA92, US06, UDDS and mixed drive cycle respectively, infer high estimation accuracy. Fig.9a, 9b, 9c and 9d shows comparative SOC estimation results for LA92, US06, UDDS and mixed drive cycle at 25^0C respectively. For the LA92 drive cycle at 25^0C, the proposed RMAEKF shows better estimation accuracy as compared to EKF, FFAEKF-I and FFAEKF-II with a minimum RMSE and MAE of 0.506% and 0.122% respectively. For the US06 drive cycle at 25^0C operating temperature, the proposed RMAEKF shows superior estimation accuracy as compared to EKF, FFAEKE-I and FFAEKF-II with a RMSE and MAE of 0.778% and 0.042% respectively. Similarly for the UDDS drive cycle at 25^0C, the proposed RMAEKF outperform other compared algorithms with a RMSE and MAE of 0.241% and 0.310% respectively. Moreover, for mixed drive cycle the proposed RMAEKF shows significant improvement in SOC estimation accuracy with a RMSE and MAE of 0.881% and 0.287% respectively, as compared to EKF, FFAEKF-I and FFAEKF-II. In EV application, high efficiency and peak charge/discharge power can be achieved at an operating temperature of $40 - 50^0$C without any damage to the battery module [28]. So, the thermal management system of the BMS is set to maintain the operating temperature of the battery module around 40^0C. From the performance indices listed in Table-3, it can be observed that at 40^0C the proposed RMAEKF gives better estimation accuracy than EKF, FFAEKF-I and FFAEKF-II with an RMSE of 0.270%, 0.928%, 0.392% and 0.925% for LA92, US06, UDDS and mixed drive cycle respectively.

B. SOC ESTIMATION WITH INCORRECT INITIAL SOC VALUE

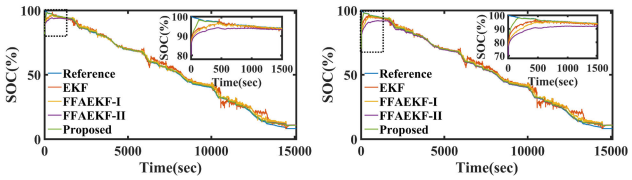

FIGURE 11. Estimated SOC result for Mixed drive cycle at 25^0C: (a) 20% SOC initialization error, (b) 30% SOC initialization error.

In this section, the performance of the proposed RMAEKF is examined under the influence of error in initialization of SOC value by setting an SOC initialization error of 20% and 30% respectively. Further, the SOC estimation accuracy of the proposed RMAEKF is evaluated and compared with EKF [27], FFAEKF-I [16], and FFAEKF-II [15]. The results are shown in Fig.11 and listed in Table-4.

- **SOC estimation with 20% error in initial value:** As mentioned in Table-2, the actual initial SOC of the battery is 100%. To check the efficacy of the proposed RMAEKF, the initial value of SOC is set to 80%

i.e. an initialization error of 20% is introduced. From the statistical analysis listed in Table-4, it is observed that with a 20% SOC initialization error, the proposed RMAEKF have a RMSE of 1.078% which is 1.467% less than EKF, 0.953% less than FFAEKF-I and 0.484% less than FFAEKF-II.

- **SOC estimation with 30% error in initial value:** Similarly, the initial SOC value is set to 70% i.e. an initialization error of 30% is applied to RMAEKF, FFAEKF-I, FFAEKF-II an EKF to compare the superiority of the proposed method. From Table-4, it is observed that, with an 30% SOC initialization error, the proposed RMAEKF outperform EKF, FFAEKF-I and FFAEKF-II with a minimized RMSE error of 1.347%.

TABLE 4. RMSE of estimated SOC with error initialization at 25^{0}C for Mixed drive cycle.

Current Profile	Methods	20% initial error	30% initial error
Mixed	EKF	2.545	2.739
	FFAEKF-I	2.031	2.610
	FFAEKF-II	1.562	2.512
	Proposed	**1.078**	**1.347**

C. SOC ESTIMATION WITH ERROR IN INITIALIZATION OF PROCESS AND MEASUREMENT NOISE COVARIANCE

In EKF-based SOC estimation, the selection of P_k and M_k depends upon how much the filter trusts in the model prediction and measurements. A high value of M implies the filter expects a higher noise level in measurement and a high value of P means the filter expects a large variation in state transition. In this work, the P_0 and M_0 are set with a value as listed in Table-2. These values may be smaller or larger as compared to the exact noise covariance values. This uncertainty in the noise covariance value may affect the performance of the proposed RMAEKF. So, to examine the performance of proposed RMAEKF in SOC estimation under the aforementioned condition. small (i.e. P_{small} and M_{small}) and large (i.e. P_{big} and M_{big}) values of noise covariance matrices are chosen from Table-2 for initialization purpose. The SOC estimation accuracy of the proposed RMAEKF is

TABLE 5. RMSE (%) of estimated SOC under current profile of Mixed drive cycle at 25^{0}C for different initial value of P and M.

Method	RMSE (%)			
	P_{small}, M_{small}	P_{small}, M_{big}	P_{big}, M_{big}	P_{big}, M_{Small}
EKF	1.595	1.641	2.441	6.518
FFAEKF-I	1.471	1.697	1.978	1.828
FFAEKF-II	1.011	0.991	1.011	1.015
Proposed	**0.894**	**0.864**	**0.877**	**0.894**

verified by comparing its RMSE with EKF, FFAEKF-I and FFAEKF-II, while considering different combinations of P and M values during initialization of the filter algorithm.

The estimated SOC results are shown in Fig.12 and corresponding statistical analysis is listed in Table-5. From Table-5 it is observed that, the proposed RMAEKF shows better estimation accuracy than other compared algorithms

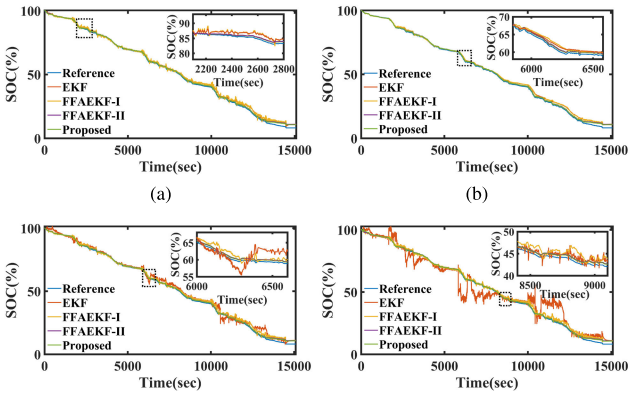

FIGURE 12. Estimated SOC result for Mixed drive cycle at 25^{0}C: (a) P_{small} & M_{small}, (b) P_{small} & M_{big}, (c) P_{big} & M_{big}, (d)P_{big} & M_{small}.

with RMSE of 0.894% for P_{small} and M_{small}, 0.864% for P_{small} and M_{big}, 0.877% for P_{big} and M_{big}, and 0.894% for P_{big} and M_{small}.

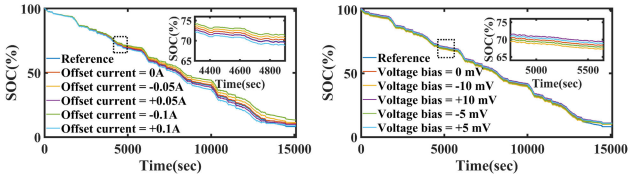

FIGURE 13. Estimated SOC result for Mixed drive cycle at 25^{0}C: (a) in presence of offset current, (b) in presence of bias voltage.

D. SOC ESTIMATION IN PRESENCE OF MEASUREMENT BIAS

During online SOC estimation, the presence of offset current and voltage bias in BMS sensor leads to an erroneous estimation of SOC due to large terminal voltage estimation error. Considering the aforementioned faulty operating condition, the efficacy of the proposed RMAEKF is examined by incorporating offset current and voltage bias with actual measured current and terminal voltage as shown in (41) and (42).

$$I_B = I_{meas} + I_{offset} \tag{41}$$

$$V_T = V_{meas} + V_{bias} \tag{42}$$

To verify the effectiveness of the proposed RMAEKF in the presence of measurement bias, current profile of mixed drive cycle at 25^{0}C is considered. Further, a current offset of $\pm$0.1A and $\pm$0.05A and a voltage bias of $\pm$10mV and $\pm$5mV are incorporated with the actual drive cycle data. The SOC estimation results in the presence of current offset and voltage bias are shown in Fig.13a and 13b respectively. The performance indices for EKF, FFAEKF-I, FFAEKF-II and the proposed RMAEKF in the presence of offset current and voltage bias are listed in Table-6. From Table-6, it can be observed that the proposed RMAEKF shows an average estimation accuracy of 1.96% and 1.56% in the presence

TABLE 6. RMSE (%) of estimated SOC for current profile of Mixed drive cycle at 25^0C in presence of offset current and bias voltage.

Current Profile	I_{offset}	RMSE (%)	V_{bias}	RMSE (%)
Mixed	- 0.1 A	1.465	-10 mV	0.856
	+ 0.1 A	3.662	+ 10 mV	1.797
	- 0.05 A	0.452	- 5 mV	0.660
	+ 0.05 A	2.262	+ 5 mV	1.313

of offset current and bias voltage respectively. Moreover, it can be observed that the impact of offset current and bias voltage is more prominent on the estimation accuracy while the battery is operating in its lower SOC range. Hence, it is recommended to operate the battery in the SOC range of 20-80% for better estimation accuracy as well as for longer battery life [29].

TABLE 7. RMSE(%) in SOC estimation due to battery capacity degradation at 0^0C, 25^0C and 40^0C for Mixed drive cycle current profile.

C_B	Temp.	EKF	FFAEKF-I	FFAEKF-II	RMAEKF
4.81Ah	0^0C	7.777	6.099	2.915	**2.471**
	25^0C	2.446	1.786	1.01	**0.881**
	40^0C	1.845	1.797	1.097	**0.925**
4.71Ah	0^0C	6.876	5.27	1.92	**1.5**
	25^0C	3.39	2.886	2.886	**2.002**
	40^0C	2.994	2.947	2.212	**2.037**
4.58Ah	0^0C	5.72	4.285	0.764	**0.668**
	25^0C	4.845	4.446	3.705	**3.584**
	40^0C	4.588	5.542	3.798	**3.626**

E. EFFECT OF TEMPERATURE VARIATION AND BATTERY CAPACITY DEGRADATION ON PROPOSED RMAEKF

The battery capacity (C_B) degrades due to cyclic aging and calendar aging [30]. In this work, three values of battery capacities, such as 4.81Ah, 4.71Ah and 4.58Ah are considered to represent the degradation of capacity due to the aging effect. Further, RMSE in SOC estimation due to capacity degradation are obtained by applying EKF, FFAEKF-I, FFAEKF-II and the proposed RMAEKF with mixed drive cycle at 0^0C, 25^0C and 40^0. The performance indices of the aforementioned SOC estimation algorithms are listed in Table-7. From Table-7, it is observed that with degradation in battery capacity and with change in temperature, the proposed RMAEKF exhibits superior performance as compared to EKF, FFAEKF-I and FFAEKF-II with the least RMSE.

F. ROBUSTNESS ANALYSIS OF PROPOSED RMAEKF

In this section, the robustness of the proposed RMAEKF is examined by incorporating all the aforementioned faulty conditions, i.e., incorrect initialization of SOC and noise covariance, presence of offset current and bias voltage at the same time. For the proposed robustness analysis, mixed drive cycle current profile at 25^0C along with 20% error in the initial SOC value, P_{big} and M_{big} as noise covariance, an offset current of +0.1A and a bias voltage of +10mV are considered. The estimated SOC and corresponding SOC error results are shown in Fig.14. Moreover, the performance

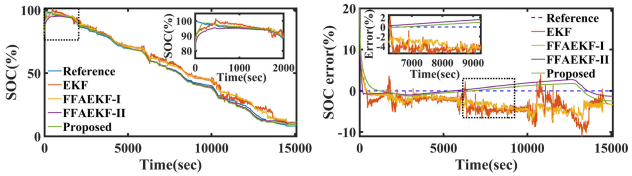

(a) (b)

FIGURE 14. Comparative robustness analysis in SOC estimation for Mixed drive cycle at 25^0C: (a) estimated SOC, (b) SOC estimation error.

indices (RMSE and MAE) are listed in Table-8. The result of robustness analysis indicates that with a RMSE of 4.483%, the proposed RMAEKF have superior performance as compared to EKF, FFAEKF-I and FFAEKF-II. Further, it implies that the proposed RMAEKF can handle bias in sensor measurement and perform better under erroneous initialization of state and noise covariance.

TABLE 8. RMSE & MAE of estimated SOC at 25^0C for current profile of Mixed drive cycle under faulty working condition.

Current Profile	Methods	RMSE(%)	MAE (%)
Mixed	EKF	8.657	20
	FFAEKF-I	8.416	20
	FFAEKF-II	5.152	20
	Proposed	**4.483**	**20**

G. COMPUTATIONAL COST AND MATRIX OPERATION COMPLEXITY ANALYSIS OF THE PROPOSED RMAEKF

TABLE 9. Mean Execution Time (T_{ME}) comparision between EKF, FFAEKF and RMAEKF.

Current Profile	T_{ME} in seconds			
	EKF	FFAEKF-I	FFAEKF-II	Proposed
Mixed	4.25	4.30	4.30	4.31

The evaluation of mean execution time (T_{ME}) helps to determine the computational cost of a SOC estimation algorithm during real-time BMS implementation [31]. The T_{ME} of an algorithm can be evaluated as per (43).

$$T_{ME} = \frac{1}{n}\sum_{i=1}^{n}(T_{ME})_i;\ i = 1, 2 \ldots .n \tag{43}$$

In this work, the computing power of an Intel(R) Core(TM) i3-6006U CPU @ 2.00 GHz processor along with MATLAB2021a version, is used for the execution of EKF, FFAEKF (I $ II) and the proposed RMAEKF. Moreover, the aforementioned algorithms are executed for i = 1, 2,...10 under the current profile of mixed drive cycle at 25^0C and the T_{ME} is evaluated and listed in Table-9. From Table-9, it is observed that both FFAEKF (I & II) and proposed RMAEKF have approximately the same T_{ME} of 4.30 sec and 4.31 sec respectively. On the other hand, due to the absence of an adaptive correction step for noise covariance matrices, EKF takes a T_{ME} of 4.25 sec which is around 0.06 sec less as compared to FFAEKF and RMAEKF.

TABLE 10. Step-wise Matrix computational complexity of the proposed RMAEKF depending upon n, m, p.

Equation	Variable	Calculation	M(n,m,p)	A(n,m,p)
(3)	$S_{k\|k-1}$	$G_{k-1}S_{k\|k-1}$	n^2	n^2-n
		$H_{k\|k-1}c_{k-1}$	np	$np-n$
		$G_{k-1}S_{k\|k-1}+H_{k\|k-1}c_{k-1}$	0	n
(4)	$E_{k\|k-1}$	$E_{k-1\|k-1}G_k^T$	n^3	n^3-n^2
		$G_kE_{k-1\|k-1}G_k^T$	n^3	n^3-n^2
		$G_kE_{k-1\|k-1}G_k^T+P_{k-1}$	0	n^2
(5)	$\widehat{O_k}$	$W_kS_{k\|k-1}$	nm	$nm-m$
		V_kc_k	mp	$mp-m$
		$W_kS_{k\|k-1}+V_kc_k$	0	m
(6)	zk	$O_k-\hat{O}_k$	0	m
(8)	K_k	$W_k^TE_{k\|k-1}$	n^2m	n^2m-nm
		$W_k^TE_{k\|k-1}W_k$	nm^2	nm^2-m^2
		$W_k^TE_{k\|k-1}W_k+M_{k-1}$	0	m^2
		$(W_k^TE_{k\|k-1}W_k+M_{k-1})^{-1}$	m^3	m^3
		$W_k^TE_{k\|k-1}(W_k^TE_{k\|k-1}W_k+M_{k-1})^{-1}$	nm^2	nm^2-nm
(9)	$S_{k\|k}$	K_kz_k	nm	$nm-n$
		$S_{k\|k-1}+K_kz_k$	0	n
(10)	$E_{k\|k}$	K_kW_k	n^2m	n^2m-n^2
		$I-K_kW_k$	0	n^2
		$(I-K_kW_k)E_{k\|k}$	n^3	n^3-n^2
(21)	$\widehat{d_k}$	$\hat{S}_{k\|k}-\hat{S}_{k\|k-1}$	0	n
(22)	$\bar{d}_k$	$\beta_1\bar{d}_{k-1}$	n	0
		$\frac{1}{C_P}\hat{d}_k$	n	0
		$\beta_1\bar{d}_{k-1}+\frac{1}{C_P}\hat{d}_k$	0	n
(23)	ΔP_k	$\hat{d}_k-\bar{d}_k$	0	n
		$\left(\hat{d}_k-\bar{d}_k\right)\left(\hat{d}_k-\bar{d}_k\right)^T$	n^2	0
		$\frac{1}{C_P-1}\left(\hat{d}_k-\bar{d}_k\right)\left(\hat{d}_k-\bar{d}_k\right)^T$	n^2	0
		$E_{k\|k-1}-G_kE_{k-1\|k-1}G_k{}^T$	0	n^2
		$\frac{1}{C_P}\left(E_{k\|k-1}-G_kE_{k-1\|k-1}G_k{}^T\right)$	n^2	0
		$\frac{1}{C_P-1}\left(\hat{d}_k-\bar{d}_k\right)\left(\hat{d}_k-\bar{d}_k\right)^T+\frac{1}{C_P}\left(E_{k\|k-1}-G_kE_{k-1\|k-1}G_k{}^T\right)$	0	n^2
(24)	P_k	β_1P_{k-1}	n^2	0
		$\mid diag\left(\beta_1P_{k-1}+\Delta P_k\right)\mid$	0	n^2
(26)	$\bar{z}_k$	$\beta_2\bar{z}_{k-1}$	m	0
		$\frac{1}{C_M}z_k$	m	0
		$\beta_2\bar{z}_{k-1}+\frac{1}{C_M}z_k$	0	m
(27)	ΔM_k	$z_k-\bar{z}_k$	0	m
		$\left(z_k-\bar{z}_k\right)\left(z_k-\bar{z}_k\right)^T$	m^2	0
		$\frac{1}{C_M-1}\left(z_k-\bar{z}_k\right)\left(z_k-\bar{z}_k\right)^T$	m^2	0
		$\frac{1}{C_M}W_kE_{k\|k-1}W_k^T$	m^2	0
		$\frac{1}{C_M-1}\left(z_k-\bar{z}_k\right)\left(z_k-\bar{z}_k\right)^T-\frac{1}{C_M}W_kE_{k\|k-1}W_k^T$	0	m^2
(28)	M_k	β_2M_{k-1}	m^2	0
		$\mid diag\left(\beta_2M_{k-1}+\Delta M_k\right)\mid$	0	m^2

$$\sum M(n,m,p)=3n^3+2n^2m+5n^2+2nm^2+2nm+np+2n+m^3+4m^2+mp+2m$$
$$\sum A(n,m,p)=3n^3+2n^2m+n^2+2nm^2+np+2n+m^3+2m^2+mp+2m$$
$$TotalComplexity=\sum M(n,m,p)+\sum A(n,m,p)=6n^3+4n^2m+7n^2+4nm^2+2nm+2np+4n+2m^3+6m^2+2mp+4m$$

Apart form mean execution time, the performance of an algorithm in real-time applications can be effectively analyzed by its worst-case complexity ($big\mathcal{O}$). In a KF based algorithm, matrix complexity depends on the number of matrix multiplications (M (.)) and matrix additions (A (.)) in each step. Further, the total complexity (T (.)) of the algorithm can be evaluated by summing the total number of M (.) and A (.) in each iteration [32].

$$TotalComplexity=\sum M(n,m,p)+\sum A(n,m,p) \quad (44)$$

where, n is state vector size, m is size of measurement vector and p represents command vector size.

Table-10 shows the M(.) and A(.) involved in each step of the proposed RMAEKF, followed by T(.) as per (44). The step-wise $big\mathcal{O}$ of EKF, FFAEKF-I, FFAEKF-II and the proposed RMAEKF are listed in Table-11. Further, the T(.) and $big\mathcal{O}$ of the aforementioned algorithms are compared in Table-12. From Table-12, it is observed that all the aforementioned algorithms possess same worst-case complexity of $6n^3$. Hence, it can be inferred that, with a moderate increment in computation cost and with the same worst-case complexity, the proposed RMAEKF provides higher SOC estimation accuracy compared to EKF, FFAEKF-I and FFAEKF-II.

TABLE 11. Big $\mathcal{O}$ complexity analysis of EKF, FFAEKF and Proposed RMAEKF depending upon n, m, p.

Steps		EKF	$\mathcal{O}(.)$	FFAEKF-I	$\mathcal{O}(.)$	FFAEKF-II	$\mathcal{O}(.)$	Proposed	$\mathcal{O}(.)$
Time Update	1	$\hat{S}_{k\|k-1}$	$2n^2$	$\hat{S}_{k\|k-1}$	$2n^2$	$\hat{S}_{k\|k-1}$	$2n^2$	$\hat{S}_{k\|k-1}$	$2n^2$
	2	$E_{k\|k-1}$	$4n^3$	$E_{k\|k-1}$	$4n^3$	$E_{k\|k-1}$	$4n^3$	$E_{k\|k-1}$	$4n^3$
Measurement Update	1	$\hat{O}_k$	$2m(n+p)$	$\hat{O}_k$	$2m(n+p)$	$\hat{O}_k$	$2m(n+p)$	$\hat{O}_k$	$2m(n+p)$
	2	z_k	m	z_k	m	z_k	m	z_k	m
	3	K_k	$4nm^2$	K_k	$4nm^2$	K_k	$4nm^2$	K_k	$4nm^2$
	4	$\hat{S}_{k\|k}$	$2mn$	$\hat{S}_{k\|k}$	$2mn$	$\hat{S}_{k\|k}$	$2mn$	$\hat{S}_{k\|k}$	$2mn$
	5	$E_{k\|k}$	$2n^3/2n^2m$	$E_{k\|k}$	$2n^3/2n^2m$	$E_{k\|k}$	$2n^3/2n^2m$	$E_{k\|k}$	$2n^3/2n^2m$
Adaptive Rule Implementation	1	-	-	e_k	$2m(n+p)$	e_k	$2m(n+m+p)$	$\bar{d}_k$	n
	2	-	-	r_k	$2m(n+p)$	r_k	$2m(n+m+p)$	$\bar{d}_k$	$3n$
	3	-	-	P	$2n^2m$	P	$4nm^2$	ΔP	$5n^2$
	4	-	-	M	$5m^2$	M	$4nm^2$	P	$2n^2$
	5	-	-	-	-	-	-	$\bar{z}_k$	$3m$
	6	-	-	-	-	-	-	ΔM	$4m^2$
	7	-	-	-	-	-	-	M	$2m^2$

TABLE 12. Comparative analysis for $T(.)$ & $\mathcal{O}(.)$ of EKF, FFAEKF and Proposed RMAEKF Algorithm.

Algorithm	T(.)	$\mathcal{O}(.)$
EKF	$6n^3 + 2n^2m + 4nm^2 + 2n^2 + 4mn + ...$	$6n^3$
FFAEKF-I	$6n^3 + 2n^2m + 2n^2 + 4nm^2 + 8mn + ...$	$6n^3$
FFAEKF-II	$6n^3 + 2n^2m + 2n^2 + 12nm^2 + 8mn + ...$	$6n^3$
Proposed	$6n^3 + 4n^2m + 7n^2 + 4nm^2 + 2mn + ...$	$6n^3$

VI. REAL-TIME IMPLEMENTATION OF THE PROPOSED RMAEKF

To ensure the practicality of the proposed RMAEKF in online SOC estimation, an experimental test bench is designed as shown in Fig.15. The aforementioned test bench is built using a host computer, a FPGA based real-time simulator (OPAL-RT OP5700), a portable scope-corder (YOKOGAWA DL350), a LAN communication channel, probes (KEYSIGHT N2843A), a PCB with I/O connectors (PCB-E06-0560) and connecting wires. The real-time experimentation is initiated by designing the proposed RMAEKF model in a MATLAB/SIMULINK environment. The OPAL-RT simulator is interfaced with the host computer through the LAN cable. The model is then loaded in OP5700 real-time simulator through RT-LAB software via the host computer and executed in real-time. The analog output of the OP5700 real-time simulator is taken through PCB-E06-0560 card and the output result is tracked through KEYSIGHT N28443A probes. The tracked output signal was then recorded in the YOKOGAWA DL350 portable scope-coder for further analysis.

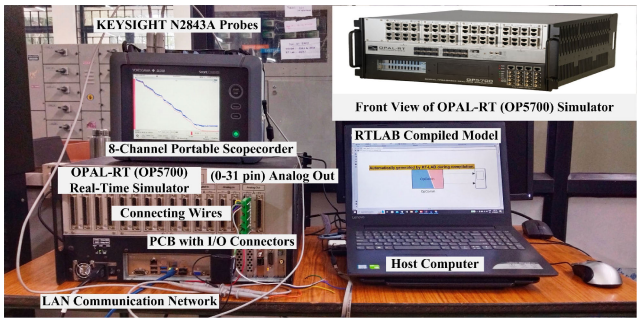

FIGURE 15. Experimental setup using OP5700 real-time simulator.

A. REAL-TIME ANALYSIS FOR EFFECT OF TEMPERATURE VARIATION

To analyze the real-time SOC estimation performance of the proposed RMAEKF under the influence of operating temperature variation, Mixed drive cycle current profiles at 0^0C, 25^0C and 40^0C are given as the input to the battery model and the corresponding estimated SOC are obtained as shown in Fig.16 a, b and c respectively. From Fig.16 it can be inferred that the proposed RMAEKF able to track the reference SOC value precisely with RMSE of 2.500% at 0^0C, 1.006% at 25^0C and 1.057% at 40^0C respectively. The comparison for estimated results of simulated and experimental SOC values are listed in Table-13.

TABLE 13. Comparative analysis for statistical result of simulated and experimental SOC at 0^0C, 25^0C and 40^0C.

Temperature	Simulated Result		Experimental Result	
	RMSE(%)	MAE(%)	RMSE(%)	MAE(%)
0^0C	2.472	5.145	2.500	5.125
25^0C	0.881	0.287	1.006	3.645
40^0C	0.925	0.249	1.057	3.883

B. REAL-TIME ROBUSTNESS ANALYSIS OF PROPOSED RMAEKF

The robustness analysis of the proposed RMAEKF in real-time application is examined by incorporating several uncertainties, such as incorrect initialization of SOC and noise covariance value, presence of bias in the terminal voltage sensor and offset in the current sensor measurement. To do so, 20% initialization error in SOC, P_{big} and M_{big} value from Table-2 are considered while initialization of the proposed algorithm. Further, an offset current of +0.1A and voltage bias of 10mV are incorporated with mixed drive cycle current at 25^0C operating temperature. The experimental results for the estimated SOC under the aforementioned uncertainty are shown in Fig.17. Further, the experimental

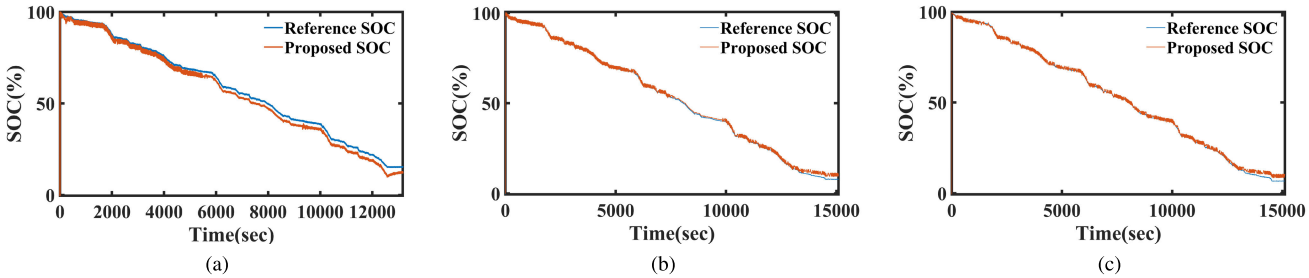

FIGURE 16. Real-time estimated SOC result for Mixed drive cycle at: (a) 0^0C (b) 25^0C, (c) 40^0C.

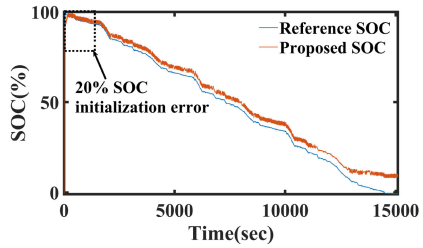

FIGURE 17. Real-time robustness analysis result for mixed current profile at 25^0C.

TABLE 14. Comparative robustness analysis of simulated and experimental SOC result for Mixed current profile at 25^0C.

Method	Simulated Result		Experimental Result	
	RMSE(%)	MAE(%)	RMSE(%)	MAE(%)
Proposed	4.483	20	4.5124	17.37

result is compared with the simulated result and listed in Table-14.

VII. CONCLUSION

This article proposes a robust modified adaptive EKF algorithm for model-based online SOC estimation of lithium batteries. From the performance analysis of the proposed algorithm, the following conclusions are obtained:

- The proposed algorithm incorporates a recursive estimation approach based on adaptive rules for iterative correction of the process and a measurement noise covariance matrix for accurate SOC estimation. The adaptive correction of the process noise covariance matrix handles the adverse effects of model uncertainty caused by the linearization of the battery model and the parametric uncertainty due to the variation in operating temperature.
- The iterative correction of the measurement noise covariance matrix improves the robustness and convergence speed in case of improper state initialization and provides high SOC estimation accuracy in the presence of offset current and voltage bias.
- The efficacy of the proposed RMAEKF is examined with the current profiles of LA92, US06, UDDS and mixed drive cycles at 0^0C, 25^0C and 40^0C operating temperatures. Further, the accuracy of SOC estimation is validated by comparing the root mean square error and maximum absolute error of the proposed RMAEKF with the performance indices of the extended Kalman filter, forgetting factor adaptive extended Kalman filter.
- The robustness of the proposed RMAEKF is examined by applying off-set current in current sensor and bias voltage to the voltage sensor of the battery.
- Furthermore, the mean execution time and computational complexity of the proposed is compared with other adaptive Kalman filters.
- Finally, a OPAL-RT simulator based real-time simulation is performed to ensure the practical applicability of the proposed RMAEKF.

The result analysis indicate robust and superior SOC estimation accuracy of proposed RMAEKF with variation in operating temperature, initialization error of SOC, and noise covariance matrices, the presence of off-set current and voltage bias as compared to other SOC estimation proposed in the literature. Moreover, the proposed RMAEKF necessitates less computational resources with low matrix operation complexity and mean execution time.

REFERENCES

[1] M. Wu, L. Qin, and G. Wu, "State of charge estimation of power lithium-ion battery based on an affine iterative adaptive extended Kalman filter," *J. Energy Storage*, vol. 51, Jul. 2022, Art. no. 104472.

[2] C. Y. Chun, B. H. Cho, and J. Kim, "Covariance controlled state-of-charge estimator of $LiFePO_4$ cells using a simplified hysteresis model," *Electrochimica Acta*, vol. 265, pp. 629–637, Mar. 2018.

[3] M. A. Hannan, M. S. H. Lipu, A. Hussain, and A. Mohamed, "A review of lithium-ion battery state of charge estimation and management system in electric vehicle applications: Challenges and recommendations," *Renew. Sustain. Energy Rev.*, vol. 78, pp. 834–854, Oct. 2017.

[4] Z. Wang, G. Feng, D. Zhen, F. Gu, and A. Ball, "A review on online state of charge and state of health estimation for lithium-ion batteries in electric vehicles," *Energy Rep.*, vol. 7, pp. 5141–5161, Nov. 2021.

[5] R. Xiong, J. Cao, Q. Yu, H. He, and F. Sun, "Critical review on the battery state of charge estimation methods for electric vehicles," *IEEE Access*, vol. 6, pp. 1832–1843, 2018.

[6] K. Qian, X. Liu, Y. Wang, X. Yu, and B. Huang, "Modified dual extended Kalman filters for SOC estimation and online parameter identification of lithium-ion battery via modified gray wolf optimizer," *Proc. Inst. Mech. Engineers, Part D, J. Automobile Eng.*, vol. 236, no. 8, pp. 1761–1774, Jul. 2022.

[7] G. L. Plett, *Battery Management Systems: Battery Modeling*, vol. 1. Norwood, MA, USA: Artech House, 2015.

[8] A. El Mejdoubi, A. Oukaour, H. Chaoui, H. Gualous, J. Sabor, and Y. Slamani, "State-of-charge and state-of-health lithium-ion batteries' diagnosis according to surface temperature variation," *IEEE Trans. Ind. Electron.*, vol. 63, no. 4, pp. 2391–2402, Apr. 2016.

[9] X. Lin, Y. Tang, J. Ren, and Y. Wei, "State of charge estimation with the adaptive unscented Kalman filter based on an accurate equivalent circuit model," *J. Energy Storage*, vol. 41, Sep. 2021, Art. no. 102840.
[10] J. Peng, J. Luo, H. He, and B. Lu, "An improved state of charge estimation method based on cubature Kalman filter for lithium-ion batteries," *Appl. Energy*, vol. 253, Nov. 2019, Art. no. 113520.
[11] G. Li, C. Liu, E. Wang, and L. Wang, "State of charge estimation for lithium-ion battery based on improved cubature Kalman filter algorithm," *Automot. Innov.*, vol. 4, no. 2, pp. 189–200, May 2021.
[12] Y. Bi and S.-Y. Choe, "An adaptive sigma-point Kalman filter with state equality constraints for online state-of-charge estimation of a Li(NiMnCo)O_2/Carbon battery using a reduced-order electrochemical model," *Appl. Energy*, vol. 258, Jan. 2020, Art. no. 113925.
[13] Z. Zhang, L. Jiang, L. Zhang, and C. Huang, "State-of-charge estimation of lithium-ion battery pack by using an adaptive extended Kalman filter for electric vehicles," *J. Energy Storage*, vol. 37, May 2021, Art. no. 102457.
[14] D. Sun, X. Yu, C. Wang, C. Zhang, R. Huang, Q. Zhou, T. Amietszajew, and R. Bhagat, "State of charge estimation for lithium-ion battery based on an intelligent adaptive extended Kalman filter with improved noise estimator," *Energy*, vol. 214, Jan. 2021, Art. no. 119025.
[15] P. Shrivastava, T. Kok Soon, M. Y. I. Bin Idris, S. Mekhilef, and S. B. R. S. Adnan, "Combined state of charge and state of energy estimation of lithium-ion battery using dual forgetting factor-based adaptive extended Kalman filter for electric vehicle applications," *IEEE Trans. Veh. Technol.*, vol. 70, no. 2, pp. 1200–1215, Feb. 2021.
[16] X. Li, Z. Wang, and L. Zhang, "Co-estimation of capacity and state-of-charge for lithium-ion batteries in electric vehicles," *Energy*, vol. 174, pp. 33–44, May 2019.
[17] N. Shi, Z. Chen, M. Niu, Z. He, Y. Wang, and J. Cui, "State-of-charge estimation for the lithium-ion battery based on adaptive extended Kalman filter using improved parameter identification," *J. Energy Storage*, vol. 45, Jan. 2022, Art. no. 103518.
[18] V. A. Bavdekar, A. P. Deshpande, and S. C. Patwardhan, "Identification of process and measurement noise covariance for state and parameter estimation using extended Kalman filter," *J. Process Control*, vol. 21, no. 4, pp. 585–601, Apr. 2011.
[19] H. Heffes, "The effect of erroneous models on the Kalman filter response," *IEEE Trans. Autom. Control*, vols. AC-11, no. 3, pp. 541–543, Jul. 1966.
[20] P. Shrivastava, T. K. Soon, M. Y. I. B. Idris, and S. Mekhilef, "Overview of model-based online state-of-charge estimation using Kalman filter family for lithium-ion batteries," *Renew. Sustain. Energy Rev.*, vol. 113, Oct. 2019, Art. no. 109233.
[21] J. Yun, Y. Choi, J. Lee, S. Choi, and C. Shin, "State-of-Charge estimation method for lithium-ion batteries using extended Kalman filter with adaptive battery parameters," *IEEE Access*, vol. 11, pp. 90901–90915, 2023.
[22] P. Kollmeyer and M. Skells, "Turnigy Graphene 5000mAh 65C Li-ion battery data," Mendeley Data, 2020, vol. 1, doi: 10.17632/4fx8cjprxm.1.
[23] F. Khanum, E. Louback, F. Duperly, C. Jenkins, P. J. Kollmeyer, and A. Emadi, "A Kalman filter based battery state of charge estimation MATLAB function," in *Proc. IEEE Transp. Electrific. Conf. Expo.*, Oct. 2021, pp. 484–489.
[24] J. Gazzarri. (2020). *Modeling Batteries Using Simulink and Simscape*. [Online]. Available: https://in.mathworks.com/videos/modeling-batteries-using-simulink-and-simscape-1562930245321.html
[25] J. Liu and X. Liu, "An improved method of state of health prediction for lithium batteries considering different temperature," *J. Energy Storage*, vol. 63, Jul. 2023, Art. no. 107028.
[26] I. Hashlamon, "A new adaptive extended Kalman filter for a class of nonlinear systems," *J. Appl. Comput. Mech.*, vol. 6, no. 1, pp. 1–12, 2020.
[27] Z. Chen, Y. Fu, and C. C. Mi, "State of charge estimation of lithium-ion batteries in electric drive vehicles using extended Kalman filtering," *IEEE Trans. Veh. Technol.*, vol. 62, no. 3, pp. 1020–1030, Mar. 2013.
[28] A. A. Pesaran, D. Swan, J. Olson, J. Guerin, S. Burch, R. Rehn, and G. D. Skellenger, *Thermal Analysis and Performance of a Battery Pack for a Hybrid Electric Vehicle*. Washington, DC, USA: National Renewable Energy Laboratory Brussels, 1998.
[29] E. D. Kostopoulos, G. C. Spyropoulos, and J. K. Kaldellis, "Real-world study for the optimal charging of electric vehicles," *Energy Rep.*, vol. 6, pp. 418–426, Nov. 2020.
[30] X. Liu, Z. Hu, X. Wang, and M. Xie, "Capacity degradation assessment of lithium-ion battery considering coupling effects of calendar and cycling aging," *IEEE Trans. Autom. Sci. Eng.*, early access, pp. 1–13, 2023, doi: 10.1109/TASE.2023.3274635.
[31] M. Lucu, E. Martinez-Laserna, I. Gandiaga, and H. Camblong, "A critical review on self-adaptive Li-ion battery ageing models," *J. Power Sources*, vol. 401, pp. 85–101, Oct. 2018.
[32] X. Tang, G. Falco, E. Falletti, and L. L. Presti, "Complexity reduction of the Kalman filter-based tracking loops in GNSS receivers," *GPS Solutions*, vol. 21, no. 2, pp. 685–699, Apr. 2017.

SATYAPRAKASH ROUT (Student Member, IEEE) received the B.Tech. and M.Tech. degrees in electrical engineering from the Biju Pattnaik University of Technology, Odisha, in 2009 and 2014, respectively. He is currently pursuing the Ph.D. degree in electrical engineering with Vellore Institute of Technology, Tamil Nadu, India. From 2013 to 2021, he was an Assistant Professor with DRIEMS University, Odisha, India. He is also a Teaching cum Research Assistant with the School of Electrical Engineering, Vellore Institute of Technology. His research interests include battery management system and battery modeling and state estimation for battery driven systems.

SATYAJIT DAS received the master's degree in electrical engineering from the National Institute of Technology, Silchar, India, in 2013, and the Ph.D. degree in electrical engineering from the National Institute of Technology (NIT), Rourkela, India, in 2019. He is currently an Assistant Professor with the School of Electrical Engineering, Vellore Institute of Technology, Tamil Nadu, India. His current research interests include power electronics, control of the wind energy systems, harmonic compensation with active power filter, and battery management systems.